Design of compact microstrip low pass filter using triangular and rectangular shaped resonator with ultra-wide stopband and sharp roll-off

Meisam Tahmasbi[1] · Farhad Razaghian[1] · Sobhan Roshani[2]

Abstract

In this paper a new microstrip lowpass filter (LPF) is designed and fabricated with sharp roll-off and ultra-wide stop-band. To obtain these features, triangular and T-shaped resonators are utilized. The main resonator is created by two triangular and rectangular shaped structures. LC equivalent circuit and transfer function of the main resonator is extracted to compute transmission zeros of the main resonator. The proposed LPF has a 3 dB cut-off frequency of 1.663 GHz. The occupied size of the designed filter is 209.33 mm^2 (17.3 mm × 12.1 mm). The ultra-wide stopband is achieved from 1.81 to 29.4 GHz with better than 20 dB attenuation. The achieved figure-of-merit of the proposed LPF is 33,813, which shows good specifications of the filter.

Keywords Lowpass filter · Sharp roll-off · Transfer function · Ultra-wide stopband

1 Introduction

Planar microwave low pass filters (LPFs) with flat and low loss passband, sharp transition band and ultra wide stop-band have attracted considerable attention in recent years. Moreover, in the modern wireless applications, apart from good frequency response, the dimension of a filter is also an important issue [1]. Filters are frequently required in many RF and microwave wireless applications [2, 3], such as diplexers, power dividers [4–6], power dividers [7] and power amplifiers [8].

So far, LPFs with wide stopband, which utilize mean-dered lines and radial patches have been presented [9, 10], but the frequency responses of the transition band were not sufficiently sharp in these works. To obtain sharp transition band, an LPF using the symmetrical T-shaped and U-shaped resonators has been reported in [11], which

shows a sharp response but this filter is rather large. LPFs using stepped impedances and hairpin resonators were proposed in [12, 13]. However, they have inappropriate size and insertion loss. Another filter with wide stopband and sharp roll-off using circular-shaped patches and open stubs was presented in [14], but the designed structure was asymmetric.

An LPF using high impedance lines and T-structured resonators is presented in [15]. The overall size of this filter is very compact and the insertion loss is acceptable, how-ever, the suppression band of this LPF is not ultra wide.

In this paper, a new compact LPF with ultra wide stopband is designed. The designed LPF shows good specifications, compared to the recent works.

2 Main resonator

The layout and frequency response of the presented trian-gular resonator are illustrated in Fig. 1. As seen in Fig. 1(b), the resonator can generate a transmission zero at 3.2 GHz, with high attenuation value.

To obtain the LC equivalent circuit (LCEC) of the presented triangular resonator, the LCECs of some typical transmission lines should be discussed at first. The LCEC

✉ Farhad Razaghian
Razaghian@azad.ac.ir

1 Department of Electrical Engineering, South Tehran Branch, Islamic Azad University, Tehran, Iran

2 Department of Electrical Engineering, Kermanshah Branch, Islamic Azad University, Kermanshah, Iran
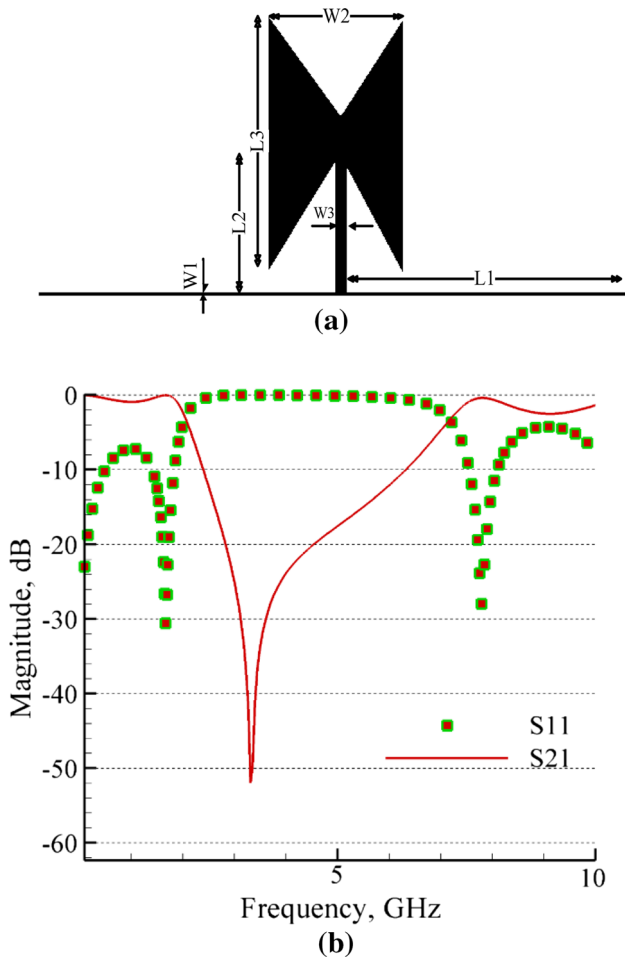
Fig. 1 a Layout structure, **b** frequency response of the triangular resonator

for a typical transmission line and an open-ended stub are illustrated in Fig. 2(a, b) [1].

The equivalent elements of the presented LCEC can be recognized by using Fig. 2 equalizing procedures. The LCEC of the triangular resonator is shown in Fig. 3.
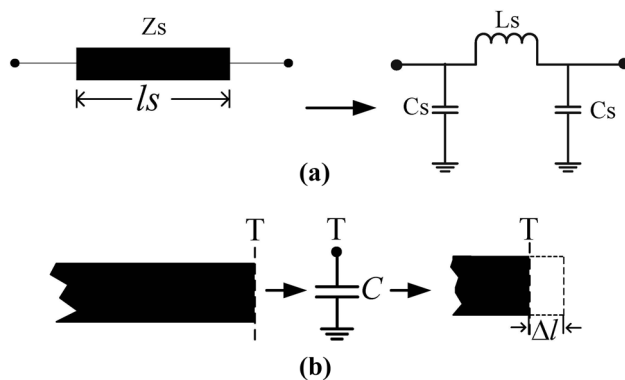

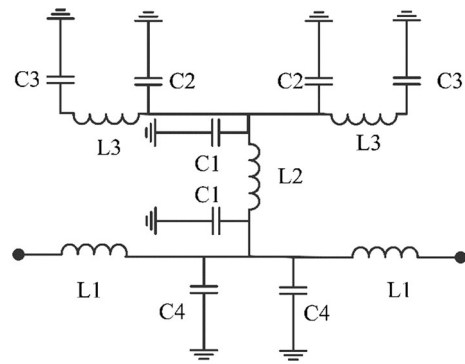**Fig. 2** The LCEC for **a** atypical transmission line, **b** an open-ended stub

Fig. 3 The LCEC of the proposed triangular resonator

In the presented LCEC, C4 and L1 are corresponding to the capacitance and inductance of the transmission line. Besides, C1, C2 and L2, L3 are capacitances and inductances of high impedance lossless line. It can be seen that Ls and Cs are elements in π-equivalent circuit. The calculated values for elements in the π-equivalent circuit using Eqs. (1) and (2) are summarized in Table 1.

$$L_{s} = \frac{1}{\omega} \times z_{s} \times \sin\left(\frac{2\pi}{\lambda_{g}} l_{s}\right) \tag{1}$$

$$C_{s} = \frac{1}{\omega} \times \frac{1}{z_{s}} \times \tan\left(\frac{\pi}{\lambda_{g}} l_{s}\right) \tag{2}$$

where ω is the angular frequency, z_s is characteristic impedance, l_s denotes length, and λ_g is the guided wavelength. The equivalent capacitance of the open-circuited stub line [Fig. 2(b)] is given as [1]:

$$C_{p} = \frac{\Delta l \cdot \sqrt{\varepsilon_{re}}}{c \cdot Z_{s}} \quad \Delta l = \frac{\xi_{1}\xi_{3}\xi_{5}}{\xi_{4}} \cdot h \tag{3}$$

where ε_{re} is the effective dielectric constant and c is the light velocity in the free space. Also, ξ_1, ξ_2, ξ_3, ξ_4 and ξ_5 are given below:

$$\xi_{1} = 0.434907 \frac{\varepsilon_{re}^{0.81} + 0.26(W/h)^{0.8544} + 0.235}{\varepsilon_{re}^{0.81} - 0.189(W/h)^{0.8544} + 0.87} \tag{4}$$

$$\xi_{2} = 1 + \frac{(W/h)^{0.371}}{2.3\varepsilon_{r} + 1} \tag{5}$$

$$\xi_{3} = 1 + \frac{0.5274 \tan^{-1}\left[0.084(W/h)^{1.9413/\xi_{2}}\right]}{\varepsilon_{re}^{0.9236}} \tag{6}$$

$$\xi_{4} = 1 + 0.037 \tan^{-1}\left[0.067(W/h)^{1.456}\right] \\ \cdot \{6 - 5\exp[0.036(1 - \varepsilon_{r})]\} \tag{7}$$

$$\xi_{5} = 1 - 0.218 \exp(-7.5W/h) \tag{8}$$

The dimensions of the triangular resonator in Fig. 1(a) are calculated as follows: W1 = 0.1, L1 = 8.5, W2 = 4.1, L2 = 4, W3 = 0.3 and L3 = 7.1 (all in millimeter). The

Table 1 Calculated values for LCEC of the proposed triangular resonator

Parameters	L1	L2	L3	C1	C2	C3	C4
Values	6 nH	1.89 nH	0.464 nH	0.18 Pf	0.057 PF	430 fF	0.21 PF

capacitance and inductance values of the equivalent circuit, which was shown in Fig. 3, can be approximated by the Eqs. (1–8) as listed in Table 1.

The electromagnetic (EM) simulation and LCEC results of the triangular resonator are compared in Fig. 4. As seen, the LCEC results of the triangular resonator and the EM simulation are in good agreement as shown in Fig. 3.

To improve the sharpness and pass band of the triangular shaped resonators, two rectangular shaped resonators are inserted in the structure to form the main resonators as shown in Fig. 5(a). The applied dimensions of the rectangular shaped resonators are as follows: Wa4 = 2.4 and La4 = 2.4 (all in millimeter).

The frequency response of the main resonator is depicted in Fig. 5(b). As seen, better pass band and sharper transition band are obtained, compared to the triangular resonator response. The LCEC of the proposed main resonator is extracted similar to triangular resonator as shown in Fig. 6.

The calculated parameters of the main resonator LCEC are summarized in Table 2. The parameters C5 and L1 are corresponding to the capacitance and inductance of the transmission line; C1, C2, C3 and L2, L3 are capacitances and inductances of high impedance line, respectively.

The EM simulation and LCEC results of the main resonator are compared in Fig. 7. As seen, the LCEC results and the EM simulation of the main resonator are in the good agreement.

The transfer function of the main resonator LCEC results is presented in Eq. (9). The transition band sharpness and main frequency of the LPF can be controlled by
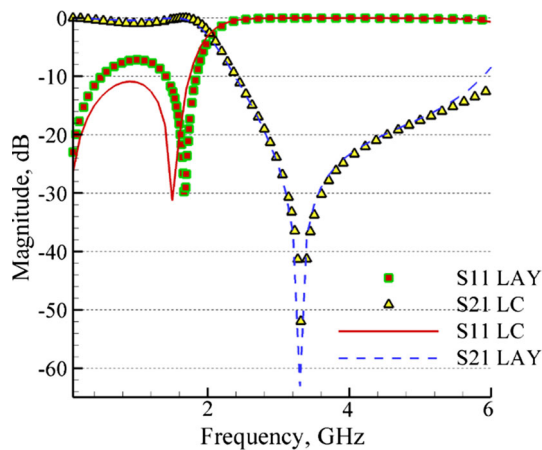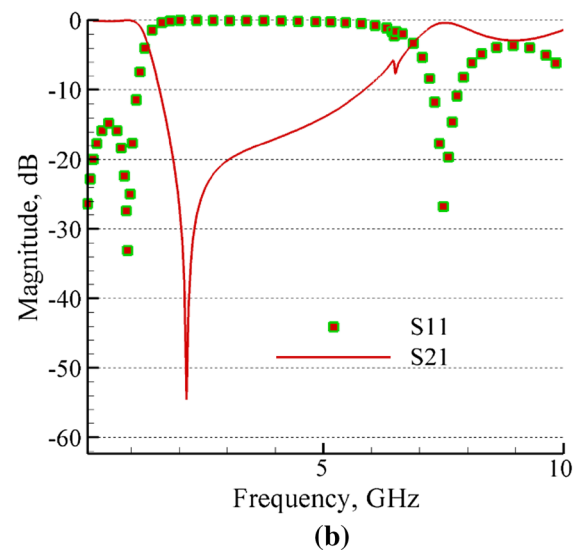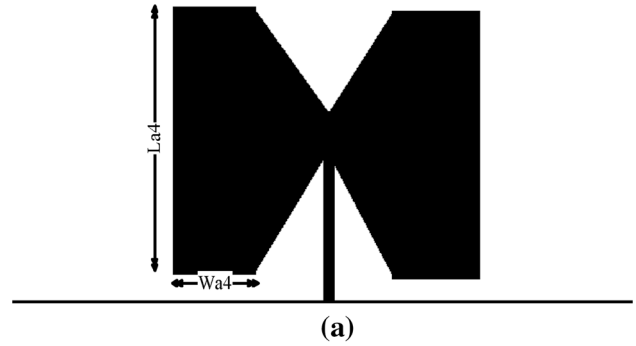

(a)

(b)

Fig. 5 **a** Structure, **b** frequency response of the main resonator

the first transmission zero. Equation of the first transmission zero is presented in Eq. (10). It should be noted that the values of r in Eq. (9) is considered 50 ohms, refers to the resistance of matching

$$\frac{V_o}{V_i} = \frac{(a^2 br)}{\begin{array}{l}(a^2 r^2 + 2abr^2 - 2a^2 bL_1 s + 2a^2 L_7 rs + 4abL_7 rs \\ + 2aL_1 r^2 s + 2bL_1 r^2 s - a^2 L_1^2 s^2 + a^2 L_7^2 s^2 + 2abL_7^2 s^2 \\ + 4aL_1 L_7 rs^2 + 4bL_1 L_7 rs^2 + L_1^2 r^2 s^2 + 2aL_1 L_7^2 s^3 \\ 2bL_1 L_7^2 s^3 + 2L_1^2 L_7 rs^3 + L_1^2 L_7^2 s^4)\end{array}}$$

(9)

where a and b parameters are defined as follows

Fig. 4 A comparison between EM simulation and LCEC results of the triangular resonator

$$
\begin{aligned}
a &= \frac{\begin{aligned}(s(c_1 + c_2 + 2(c_3 + c_4) + (c_2(c_3 + c_4)L_3 \\ + (c_2 + 2c_3)c_4L_4 + c_1(c_2L_2 + (c_3 + c_4)(2L_2 + L_3) \\ + c_4L_4))s^2 + (c_1c_2(c_3 + c_4)L_2L_3 + c_4(c_1(c_2 + 2c_3)L_2 \\ + (c_1 + c_2)c_3L_3)L_4)s^4 + c_1c_2c_3c_4L_2L_3L_4s^6))\end{aligned}}{\begin{aligned}(1 + s^2(c_4(2L_2 + L_3 + L_4) + c_3(2L_2 + L_3)(1 + c_4L_4s^2) \\ + c_2L_2(1 + (c_3L_3 + c_4(L_3 + L_4))s^2 + c_3c_4L_3L_4s^4)))\end{aligned}} \\[2mm]
b &= \frac{(1 + c_5L_5s^2 + c_6L_5s^2 + c_6L_6s^2 + c_5c_6L_5L_6s^4)}{\begin{aligned}((2c_5s + 2c_6s + c_7s + c_5c_7L_5s^3 + c_6c_7L_5s^3 \\ + 2c_5c_6L_6s^3 + c_6c_7L_6s^3 + c_5c_6c_7L_5L_6s^5))\end{aligned}}
\end{aligned}
$$

$$
T_Z = \sqrt{\begin{aligned}&\frac{-C}{3D} - \frac{2^{1/3}B}{\left(-2C^3 + 9BCD - 27AD^2 + \left(\sqrt{4(-C^2 + 3BD)^3 + (-2C^3 + 9BCD - 27AD^2)^2}\right)\right)^{1/3}} \\[2mm] &+ \frac{2^{1/3}C^2}{3D\left(-2C^3 + 9BCD - 27AD^2 + \left(\sqrt{4(-C^2 + 3BD)^3 + (-2C^3 + 9BCD - 27AD^2)^2}\right)\right)^{1/3}} \\[2mm] &\frac{\left(\pm 2C^3 + 9BCD - 27AD^2 + \left(\sqrt{4(-C^2 + 3BD)^3 + (-2C^3 + 9BCD - 27AD^2)^2}\right)\right)^{1/3}}{32^{1/3}D}\end{aligned}}
$$

(10)

Table 2 Calculated parameters of the main resonator LCEC

Parameters	L1	L2	L3	L4	C1	C2	C3	C4	C5
Values	6 nH	1.89 nH	0.46 nH	0.83 nH	0.18 PF	0.05 PF	1.01 PF	170 fF	0.21 PF

Fig. 6 The LCEC of the main resonator

Fig. 7 EM simulation and LCEC results of the main resonator
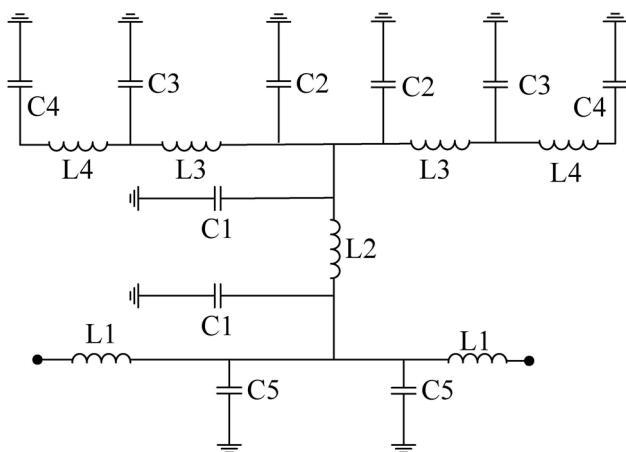
where

$A = (c_1 + c_2 + 2(c_3 + c_4) + (c_2(c_3 + c_4)L_3$

$B = (c_2 + 2c_3)c_4L_4 + c_1(c_2L_2 + (c_3 + c_4)(2L_2 + L_3) + (c_4L_4))$

$C = (c_1c_2(c_3 + c_4)L_2L_3 + c_4(c_1(c_2 + 2c_3)L_2 + (c_1 + c_2)c_3L_3)L_4)$

$D = c_1c_2c_3c_4L_2L_3L_4$

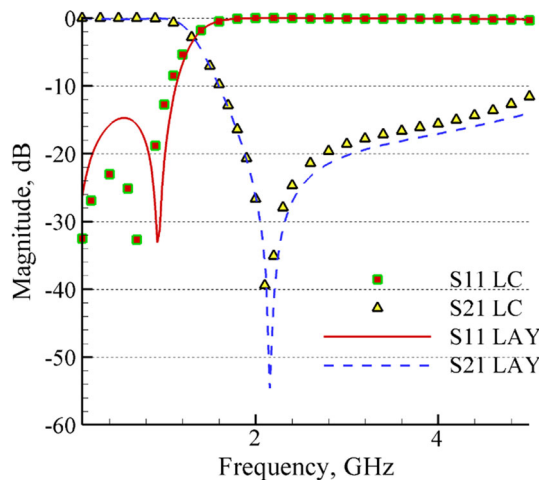For example, if L1 increases to 3.17 nH, 3.5 nH and 4 nH, the transmission zero will increase to 2.1 GHz, 2.45 GHz, and 2.68 GHz, respectively. So, L1 can be used to control transmission zero. Also, the transmission zero location can be changed by C3, C4 and, L4. The mentioned
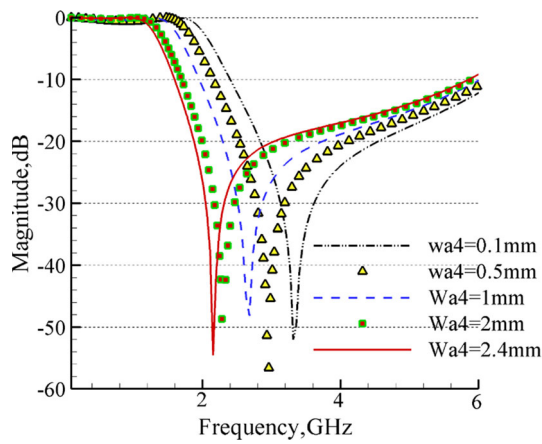
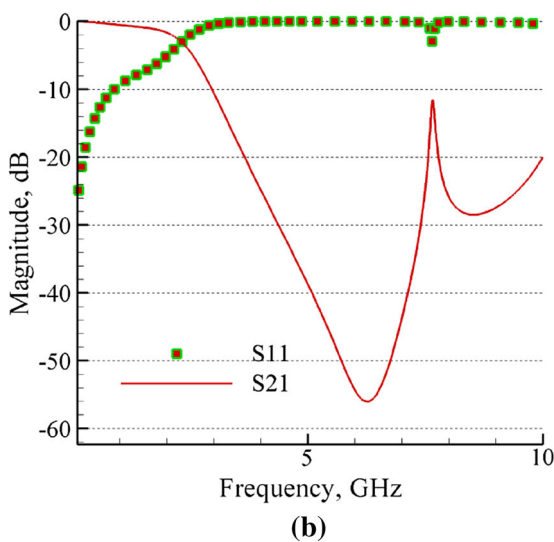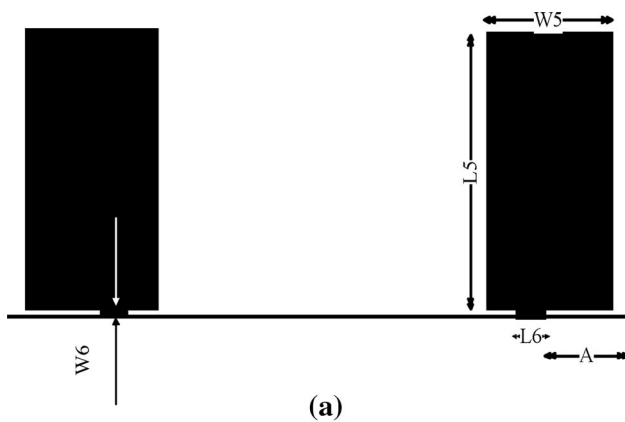**Fig. 8** The effects of the Wa4 different values on the position of transmission zero for the main resonator

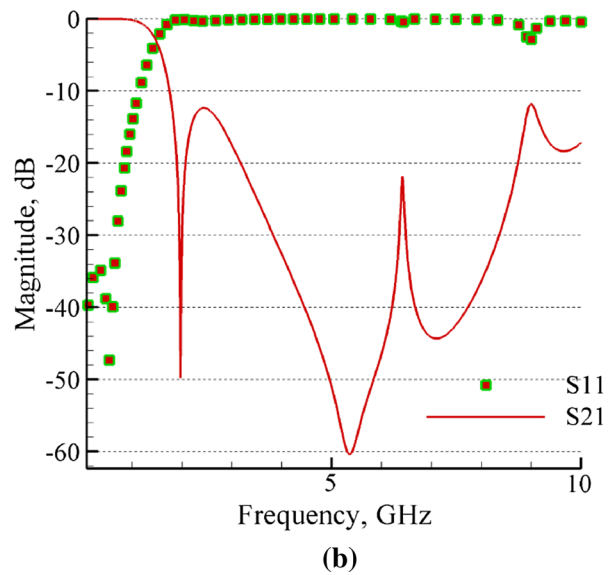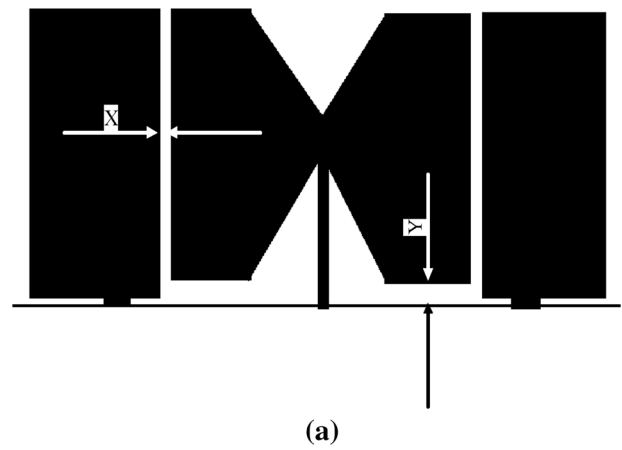**Fig. 9** **a** Layout structure, **b** frequency response of T-shaped resonator

Fig. 10 **a** Layout structure, **b** frequency response of the initial filter

lumped elements are calculated by Wa4. The effects of the Wa4 different values on the position of transmission zero for the main resonator are shown in Fig. 8. In this figure, the impact of changing the Wa4 values of 0.1, 0.5, 1, 2 and 2.4 mm, on frequency responses of the main resonator is shown. With these changes, the frequency of transmission zero is moved to 3.25, 2.9, 2.7, 2.3, 2.1 GHz and the value of C4 is changed to 14, 41, 97, 152, 170 fF, respectively.

3 Low pass filter design

T-shaped suppressor resonators are added to the main resonator to make an ultra-wide stop-band as depicted in Fig. 9(a). The frequency response of the T-shaped
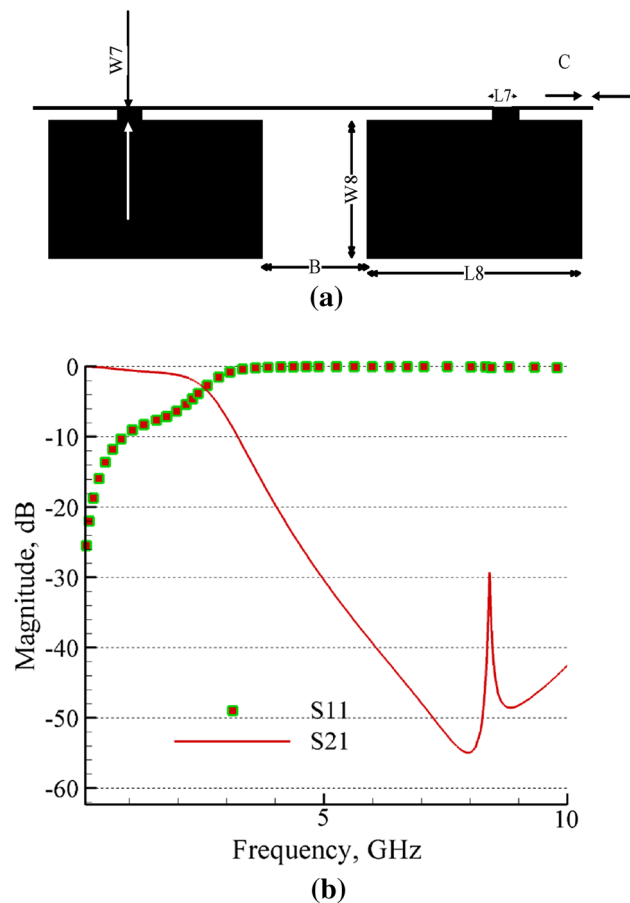
Fig. 11 a Layout structure, **b** frequency response of the second T-shaped resonator

Fig. 12 a Layout structure, **b** frequency response of the final proposed filter

resonators is illustrated in Fig. 9(b). As can be seen in this figure, some harmonics can be eliminated by the T-shaped resonators. The dimensions of the T-shaped resonator in Fig. 9(a) are as follows: W5 = 3.9, L5 = 7.5, W6 = 0.3, L6 = 0.8, A = 2.6 (All in millimeter). The frequency response of the T-shaped resonator is depicted in Fig. 9(b).

After adding the T-shaped resonators to the main resonator, the initial filter structure will be obtained which is shown in Fig. 10(a). Therefore microstrip prototype filter which is shown in Fig. 10(a) is achieved. Frequency response of this structure is depicted in Fig. 10(b). The dimensions of the prototype in Fig. 10(a) are as follows: X = 0.3 mm and Y = 0.6 mm.

There are two unwanted harmonics in the initial filter response at 2.3 GHz and 9.2 GHz. To eliminate these harmonics, another T-shaped (second T-shaped) resonator is added, which is depicted in Fig. 11(a). The frequency response of the second T-shaped resonator is illustrated in Fig. 11(b).
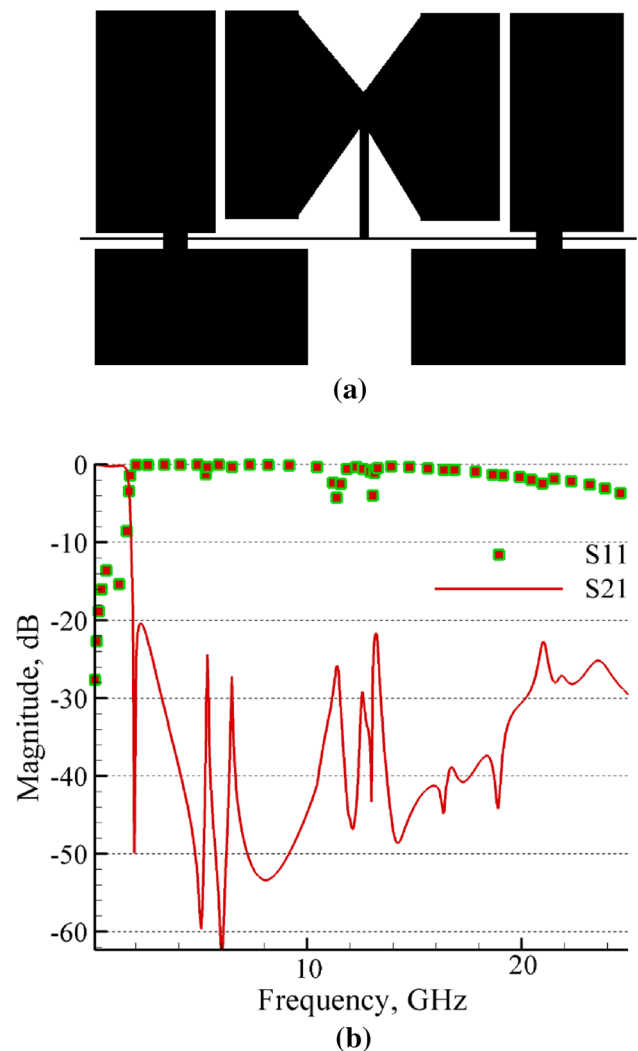
To conclude this section, the final design of microstrip filter and its frequency response are illustrated in Fig. 12(a, b).

The stopband of the proposed LPF is achieved from 1.81 to 29.4 GHz with more than 20 dB attenuation. Furthermore, the cut of frequency of the proposed LPF is 1.663 GHz. The frequency response and LCEC of the proposed LPF is depicted in Fig. 13. As seen, the LCEC results and EM simulation are in the good agreements.

The calculated values of the extracted LCEC for the proposed filter are listed in Table 3.

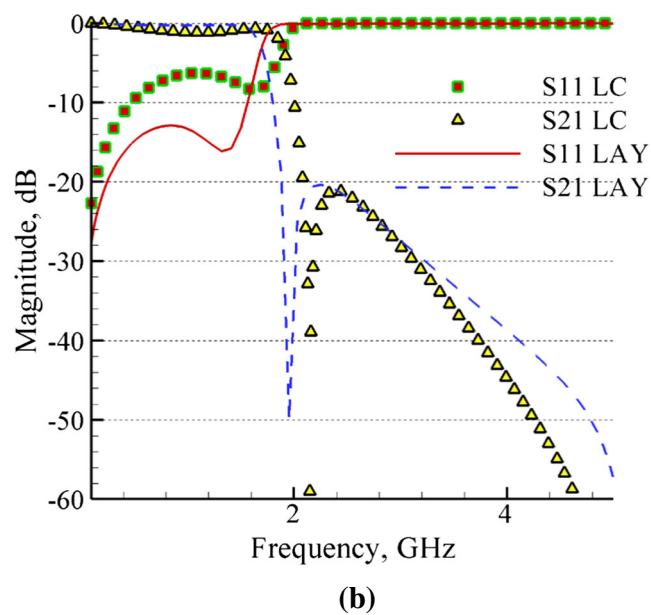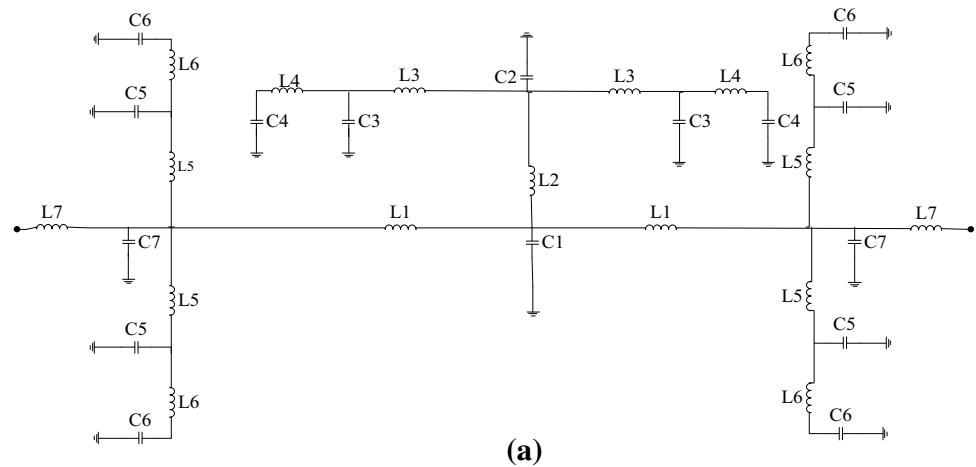**Fig. 13** **a** The LCEC, **b** the frequency response of the proposed LPF

(a)

(b)

Table 3 Calculated values of the extracted LCEC for the proposed filter

Parameters	L1	L2	L3	L4	L5	L6	L7
Values	3.17 nH	1.89 nH	0.46 nH	0.83 nH	0.3 nH	0.44 nH	1.51 nH
Parameters	C1	C2	C3	C4	C5	C6	C7
Values	0.42 PF	0.29 PF	1.01 PF	17 fF	1.82 PF	1 fF	0.11 PF

4 Simulation and measurement results

The fabricated LPF results are illustrated in Fig. 14. As seen, the measured data follow the simulation results. Also, the picture of the fabricated proposed filter is shown in Fig. 15.

A transition band from 1.663 GHz up to 1.88 GHz corresponding with 3–40 dB attenuations is achieved for the proposed LPF. The proposed LPF is fabricated on a RO-4003 substrate with a thickness of 32 mil and a dielectric constant of 3.38. The results are measured using an HP8757A vector network analyzer.
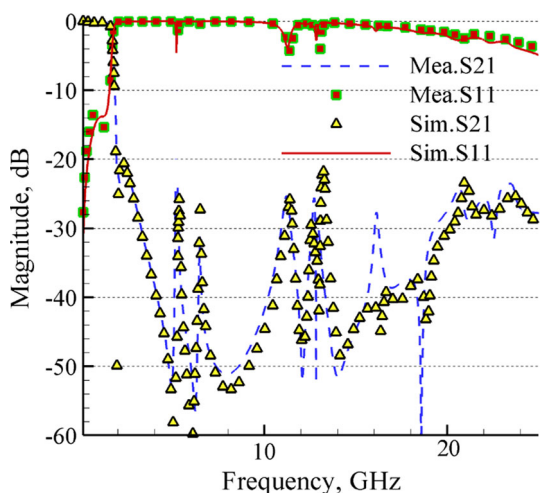
Fig. 14 The fabricated LPF results

Fig. 15 Photograph of the fabricated proposed filter

The performance of the proposed LPF is listed in Table 4, which is compared with other published paper. According to the Table 4, high figure-of-merit of 33,813 is obtained for the proposed LPF.

In the Table 4, the parameter roll-off rate denotes the transition band sharpness. Also, the parameters SF, RSB and NCS are suppression factor, relative stopband bandwidth, and normalized circuit size, respectively. The FOM can be calculated as defined in Eq. (11)

$$FOM = \frac{(\text{Roll-off rate}) \times SF \times RSB}{AF \times NCS} \quad (11)$$

where the architecture factor (AF) is considered as 1 or 2, when the design is 2D or 3D, respectively.

5 Conclusions

In this article, a compact microstrip LPF with a sharp response and ultra wide stopband is designed and fabricated. The simulation and measurement result shows a good agreement. Besides, figure-of-merit of 33,813 is obtained which is very high compared to the other reported works. The designed LPF can be applied to the modern communication systems because of the obtained good features.

Table 4 Performance comparisons between published LPFS and this work

Refs.	Roll-off rate (dB/GHz)	RSB	SF	NCS $(\lambda_g \times \lambda_g)$	AF	FOM
[16]	56.7	1.63	2	0.115×0.116	2	7109
[17]	97.4	1.87	2	0.1×0.19	1	19,172
[18]	52.8	1.52	2	0.081×0.113	1	18,475
[19]	100	1.49	2	0.255×0.131	2	9030
[20]	100	1.71	1.6	0.21×0.09	1	13,680
[21]	48.5	1.61	2	0.141×0.151	1	7436
[22]	94	1.26	2.3	0.243×0.169	1	6645
[23]	29.3	1.53	2.4	0.15×0.05	2	7172
This work	171	1.75	2	0.159×0.111	1	33,813

References

1. Hong, J. S., & Lancaster, M. J. (2004). *Microstrip filters for RF/microwave applications*. London: Wiley.
2. Verma, A. K., et al. (2011). Design of low-pass filters using some defected ground structures. *International Journal of Electronics and Communications, 65*(10), 864–872.
3. Ballam, A., et al. (2007). Quasi-elliptic microstrip low-pass filters using an interdigital DGS slot. *IEEE Microwave and Wireless Components, 17*(8), 586–588.
4. Roshani, S., & Roshani, S. (2019). Design of a very compact and sharp bandpass diplexer with bended lines for GSM and LTE applications. *AEU-International Journal of Electronics and Communications, 1*(99), 354–360.
5. Heshmati, H., & Roshani, S. (2018). A miniaturized lowpass bandpass diplexer with high isolation. *AEU-International Journal of Electronics and Communications, 1*(87), 87–94.
6. Noori, L., & Rezaei, A. (2018). Design of a compact narrowband quad-channel diplexer for multi-channel long-range RF communication systems. *Analog Integrated Circuits and Signal Processing, 94*(1), 1–8.
7. Roshani, S., Roshani, S., & Zarinitabar, A. (2018). A modified Wilkinson power divider with ultra harmonic suppression using open stubs and lowpass filters. *Analog Integrated Circuits and Signal Processing, 98,* 1–5.
8. Pirasteh, A., Roshani, S., & Roshani, S. (2018). A modified class-F power amplifier with miniaturized harmonic control circuit. *AEU-International Journal of Electronics and Communications, 1*(97), 202–209.
9. Ge, L., et al. (2010). Compact microstriplowpass filter with ultra-wide stopband. *Electronics Letters, 46*(10), 689–691.
10. Wang, J., et al. (2010). Compact quasi-elliptic microstriplowpass filter with wide stopband. *Electronics Letters, 46*(20), 1384–1385.
11. Karimi, G., et al. (2014). Design of microstrip LPF with sharp cut-off frequency and wide stopband. *Frequenz, 68*(7–8), 313–319.
12. Li, L., et al. (2010). Compactlowpass filters with sharp and expanded stopband using stepped impedance hairpin units. *IEEE Microwave and Wireless Components Letters, 20*(6), 310–312.
13. Zhang, R., et al. (2014). Design of a wideband bandpass filter with composite short-and open-circuited stubs. *IEEE Microwave and Wireless Components Letters, 24*(2), 96–98.
14. Karimi, G., et al. (2013). Design of sharp roll-off lowpass filter with ultra wide stopband. *IEEE Microwave and Wireless Components Letters, 23*(6), 303–305.
15. Pirasteh, A., Roshani, S., & Roshani, S. (2018). Compact microstrip lowpass filter with ultrasharp response using a square-loaded modified T-shaped resonator. *Turkish Journal of Electrical Engineering and Computer Sciences, 26*(4), 1736–1746.
16. Jiang, S., & Xu, J. (2017). Compact microstriplowpass filter with ultra-wide stopband based on dual-plane structure. *Electronics Letters, 53*(9), 607–609.
17. Roshani, S. (2017). A compact microstrip low-pass filter with ultra wide stopband using compact microstrip resonant cells. *International Journal of Microwave and Wireless Technologies, 9*(5), 1023–1027.
18. Liu, S., Xu, J., & Xu, Z. (2015). Compact lowpass filter with wide stopband using stepped impedance hairpin units. *Electronics Letters, 51*(1), 67–69.
19. Kumar, L., & Parihar, M. S. (2016). Compact hexagonal shape elliptical lowpass filter with wide stop band. *IEEE Microwave and Wireless Components Letters, 26*(12), 978–980.
20. Majidifar, S. (2016). High performance microstrip LPFs using dual taper loaded resonator. *International Journal for Light and Electron Optics, 127*(6), 3484–3488.
21. Sheikhi, A., Alipour, A., & Hemesi, H. (2017). Design of microstrip wide stopband lowpass filter with lumped equivalent circuit. *Electronics Letters, 53*(21), 1416–1418.
22. Raphika, P. M., Abdulla, P., & Jasmine, P. M. (2016). Planar elliptic function lowpass filter with sharp roll-off and wide stopband. *Microwave and Optical Technology Letters, 58*(1), 133–136.
23. Majidifar, S. (2016). Design of high performance miniaturized lowpass filter using new approach of modeling. *Applied Computational Electromagnetics Society Journal, 31*(1), 52–57.

Meisam Tahmasbi was born in Kermanshah, Iran in 1988. He received his B.Sc. degree in Electronic Engineering in 2010 from Islamic Azad University, Kermanshah Branch, Kermanshah, Iran, M.Sc. degree in Electrical Engineering from Islamic Azad University, Central Tehran Branch, Tehran, Iran and he is now a. Ph.D. student in Electronic Engineering in Islamic Azad University, South Tehran Branch, Tehran, Iran. His current research interests are RF/Microwave, Power amplifiers circuit design.

Farhad Razaghian received the B.Sc. and M.Sc. degrees in Electronics Engineering from Islamic Azad university South Tehran Branch, Tehran, Iran, and the Ph.D. degree in Electronics Engineering from the Islamic Azad University Science and Research Branch, Tehran, Iran. His research interests are analog circuits, CMOS integrated circuits, power amplifiers and RFIC design as well as VLSI/FPGA implementation of algorithms.

Sobhan Roshani received the B.Sc. degree in Electrical Engineering from Razi University, Kermanshah, Iran in 2010, M.Sc. degree in Electrical Engineering from Iran University of Science and Technology—IUST, Tehran, Iran in 2012 and Ph.D. in Electrical Engineering from Razi University in 2016. He has published more than 50 papers on international journals and conferences. His research interest includes switching power amplifiers, microwave circuits, optimization and neural networks.